ENGINEERING TRANSACTIONS • Engng. Trans. • 41, 3–4, 395–417, 1993
Polish Academy of Sciences • Institute of Fundamental Technological Research

ON MICROMECHANICAL MODELING OF DEFORMATION OF COMPACT ROCK IN COMPRESSION

M. BASISTA (WARSZAWA)

The paper proposes a simple two-dimensional damage model for low-porosity rocks loaded in compression. The sliding crack mechanism is selected as an underlying micromechanism of the inelastic deformation at the macroscale. A numerical example is worked out showing the capability of the model for duplicating the experimentally observed trends of rock deformation.

1. Preliminaries

The process of cracking and failure of natural geologic solids like polycrystalline rocks have attracted considerable attention over the past 3–4 decades. This ever-growing interest is rooted in practical geotechnical applications involving, as a rule, mechanical properties of rocks. Consequently, much research effort has gone into a better understanding of the microscopic mechanisms underlying the behaviour of rocks observed *in situ* or in the laboratory tests.

Rock is a heterogeneous, cohesive material containing numerous inhomogeneities such as microcracks, pores, grain boundaries, joints, second phase inclusions and other structural defects at all scales, even in the virgin state, i.e. prior to any application of loading. Under the action of externally applied stresses those flaws become stress concentrators. The stresses thus generated often lead to a further degradation of the material properties and, eventually, to the overall failure. It is well recognized that even under compressive loading the rock deformation proceeds by the growth, interaction and linkage of many tensile microcracks.

The most characteristic features accompanying a highly nonlinear and complex process of rock deformation can be briefly summarized as follows:

Pressure dependence: lateral confinement strongly affects the ultimate strength and determines the failure mode. At higher confining pressures the average crack length is reduced promoting the transition from brittle to ductile behaviour, cf. [1].

Positive dilatancy: brittle crack growth is necessarily a dilatant process involving volume increase; initial volume decrease observed in compression tests is related to the crushing of preexisting voids.

Load induced anisotropy: even though the preexisting crack population is, in all probability, randomly distributed within the material volume, their subsequent growth is a directional process depending, among other factors, on the principal stress directions.

In unconfined compressive tests the microcracks grow predominantly on the planes parallel to the direction of loading. The final fracture in the form of splitting is commonly attributed to the unstable propagation of one or more of the largest and most favorably oriented cracks running longitudinally towards specimen's ends. The failure is abrupt and inelastic strains at failure remain relatively small.

In contrast, if a substantial lateral confinement is applied, the deformation process is more complicated since it incorporates both brittle and ductile deformation modes. The final fracture (faulting) in a confined specimen results from the cooperative action of many small cracks that grow stably, interact and eventually form a dominant shear fault (crack band) at some angle to the maximum load axis. The stress-strain curve in this case visibly deviates from the straight line. The inelastic and elastic strains at failure (apex of the $\sigma - \varepsilon$ curve in the stress-controlled test) are typically of the same order of magnitude.

Microstructural parameters, such as grain size, porosity, distribution of cleavage planes, initial crack density, etc., are as vital to the process of rock deformation as the action of external loading agencies.

The microcrack growth under compression may occur according to several different mechanisms. Those mechanisms have been extensively studied and modeled analytically as well as simulated by model experiments ([1, 2, 3, 4, 5, 6, 7], etc.). Below, the most commonly used models are briefly characterized and commented upon with regard to their applicability in rock mechanics.

For rocks exhibiting high porosity (some sandstones and limestones) the micromechanism depicted in Fig. 1 is often incorporated to model the inelastic and dilatant macroscopic response. The crack nucleation is attributed

to the presence of pores. Under external compressive stresses σ_1 and low lateral pressure σ_2, tensile hoop stresses are generated at the apex of a pore (assumed to be spherical in shape). If the tensile hoop stress, further increased by a notch that is always likely to occur in a real rock, exceeds the local fracture strength of the material, the tensile microcracks initiate and grow in the direction of σ_1. The formula for the stress intensity factor that holds for both the small and large tensile crack lengths (Fig. 1) is given in [5]. A routine analysis of K_I reveals that for short crack lengths L the cracks generated by the squeezed-pore mechanism behave in an unstable manner $(\partial K_I/\partial L > 0)$ and stabilize after some crack length at which $(\partial K_I/\partial L)$ becomes negative.

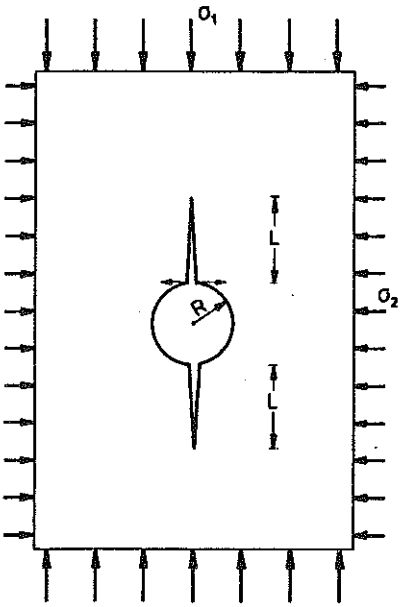

FIG. 1.

In the case of compact, or low porosity, rocks like granite, the inelastic deformation is typically attributed to the sliding (or winged) crack mechanism shown in Fig.2. This mechanism was originated by BRACE and BOMBOLAKIS [2] and pursued further in a series of papers by NEMAT-NASSER and HORII [8], KACHANOV [3], FANELLA and KRAJCINOVIC [9]. It involves a rather complex succession of events starting with the frictional sliding on the faces of preexisting (closed) flaws, followed by the out-of-plane, curvilinear kinking from the crack tips, and completed by the subsequent Mode-I growth of the kinked wings in the planes roughly parallel to the direction

of the dominant compressive stress. Depending on the sign of the confining stress, the tensile wing cracks may grow either in a stable or unstable manner. If $\sigma_2 < 0$ (lateral compression), the crack growth is stable, while even a small lateral tension ($\sigma_2 > 0$) makes it unstable. The details of the deformation process based on the sliding crack mechanism will be discussed more thoroughly later in this paper.

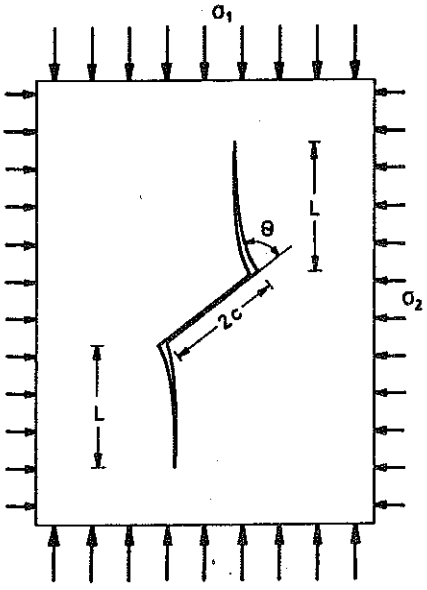

FIG. 2.

Other idealizations of brittle cracking micromechanisms in compressed rocks, based on the K_I solutions, include the elastic mismatch model (Fig.3a), the bending model (Fig. 3b) and the squeezed-grains model (Fig. 3c), just to mention only the most common ones. The elastic mismatch model assumes that tensile stresses may be generated at the interface of two elastic materials of different elastic moduli E_1, E_2. These stresses occur as a result of unequal lateral deformations of the two materials. They are often capable of nucleation of a tensile interface microcrack which further propagates in a less compliant material as sketched in Fig. 3a, [7]. According to the bending model, the tensile stresses necessary to trigger the microcrack growth result from the bending of a soft and elongated inclusion over two harder ones (Fig. 3b). The cracking mechanism depicted in Fig. 3c consists in the activation of a crack at the particle-matrix interface, driven by local tensile stresses ensuing from the lateral squeezing out of the grains in a favorable configuration [10].

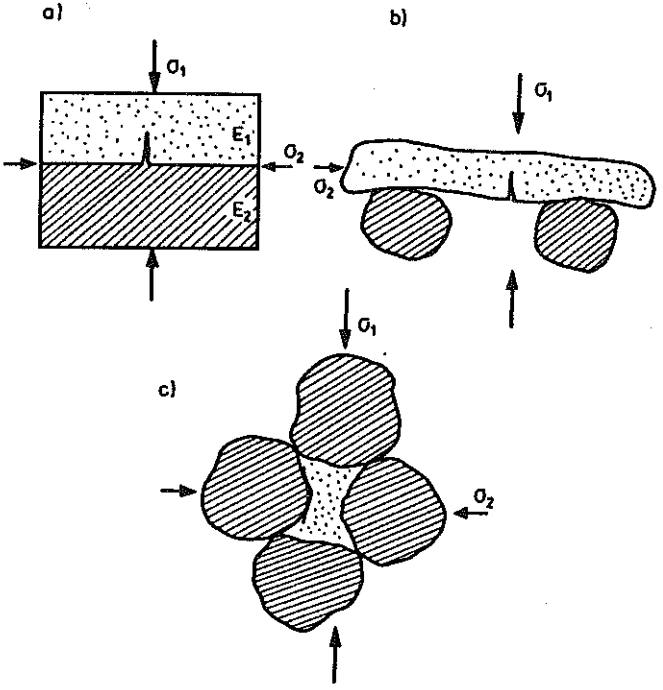

FIG. 3.

Irrespective of the micromechanism underlying the inelastic macro-deformation, a typical $\sigma - \varepsilon$ diagram of a rock specimen in the confined compression test has the form shown in Fig. 4. Points A to F correspond to the succession of different deformation phases. In the phase OA the closure of preexisting voids occurs. In the region AB a compact rock behaves like a perfectly elastic material, thus will be modeled by a straight line. The nonlinear phase BF is the macroscopic manifestation of the energy dissipating processes of frictional sliding over the preexisting crack faces (segment BC) followed by the wing crack opening (segment CF). The peak F indicates that a qualitative change took place in the microscale processes underlying the macroscopic deformation. Apparently some of the interacting microcracks joined each other to form a well-developed crack cluster (or a macrocrack) whose growth begins to contribute overwhelmingly to the overall deformation of the specimen. The final fracture in form of splitting or faulting is then imminent depending on the amount of the lateral confinement. At higher levels of lateral confinement a typical plastic behaviour is reported [11]. This is attributed to the resistive action of the lateral pressure which opposes the wing crack propagation while inflicting the plastic zones

in the vicinity of the preexisting cracks tips. Also note that the nonlinear lateral strain is substantially larger than its axial counterpart. A possible explanation of this fact will be offered later on.

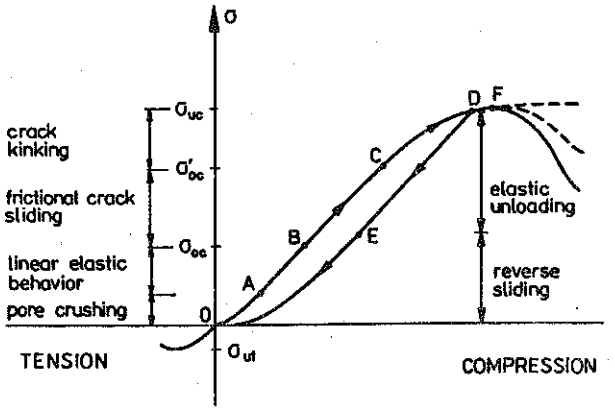

FIG. 4.

The main objective of this note is to add to the general discussion on the constitutive modeling of rocks with internal cracks by formulating a simple, two-dimensional, continuum model of the compact rock deformation in compression. The proposed model will make use of the widely referenced sliding crack mechanism (Fig. 2). The present paper is also intended as an initial effort towards the formulation of a micromechanically based phenomenological theory of brittle rock deformation. A compelling argument is thus made for simplicity of the proposed micromechanical model emphasizing the salient aspects of the deformation process at the expense of unimportant details.

2. SLIDING CRACK MECHANISM

The concept of sliding crack mechanism has been analyzed in considerable detail in the recent past (see [17] and references contained therein). Despite its wide popularity among analysts, this model was criticized by several authors on the grounds that winged cracks have rarely been identified in SEM studies of geomaterials. Instead, tensile microcracks seemed to originate at a variety of sources. However, recent data [12], [13] suggest that the focal mechanism for stress-induced acoustic emissions involves shear motions. Winged configurations were unambiguously observed in ice under compression [14]. Similar micromechanism exists in semi-brittle ceramics [15]. It is therefore accepted, or even advocated, in this paper that

the general concept of a frictional sliding crack constitutes at least one major micromechanism of inelasticity under compression in the elastic-brittle range of behaviour.

For the sake of clarity, select a representative initial microdefect as a single, closed, rectilinear crack (slit) of the length $2c$ making an angle $\gamma = 45°$ with the directions of the principal stresses σ_1, σ_2, Fig. 5a. The sign convention adopted here labels compressive stresses negative. It is further assumed that $|\sigma_1| > |\sigma_2|$.

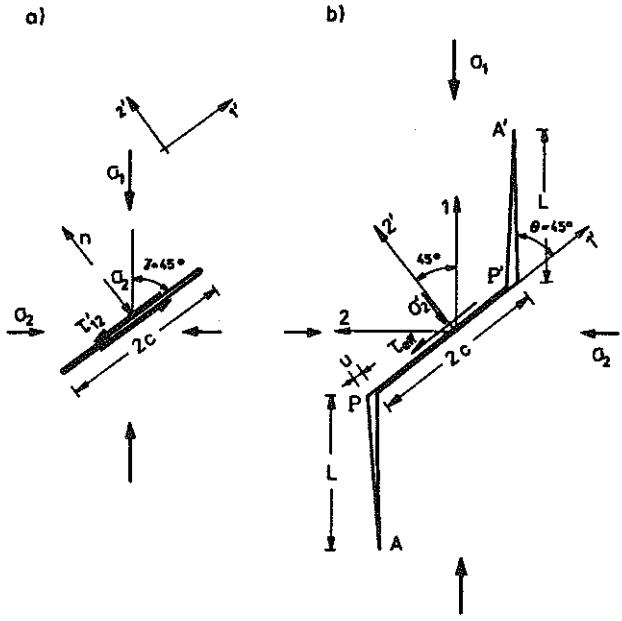

FIG. 5.

The onset of inelastic deformation is typically attributed to the initiation of frictional sliding over the faces of the preexisting cracks. During this phase the cracks retain their length $2c$, thus no new internal surfaces are created. The only energy dissipating mechanism is then the frictional sliding in the shearing mode. It is also assumed that the inclined preexisting crack remains closed during the whole deformation process. The sliding commences when the resolved shear stress τ_{12} acting on the crack faces exceeds the frictional and cohesive resistance of the matrix material, i.e.

$$\tau_{\text{eff}} = \tau_{12} + \mu\sigma'_2 - \tau_c > 0. \tag{2.1}$$

In (2.1) τ_{eff} denotes an effective shear, $\tau_{12} = \frac{1}{2}\sin 2\gamma(\sigma_1 - \sigma_2)$ is the resolved shear, and $\sigma'_2 = \sigma_1 \sin^2\gamma + \sigma_2 \cos^2\gamma$ the normal stress in the local coordinate

system; μ is the coefficient of friction (positive constant), and τ_c the cohesive resistance of the material. A rigorous analysis requires a rational, experimentally based estimate of the cohesive resistance τ_c with the increasing slip of the crack faces. It is reported in the literature (e.g. [4]) that τ_c actually decays and eventually disappears as the slip on the preexisting crack accumulates. However, in the absence of a commonly accepted relationship it is postulated as the simplest solution that τ_c remains constant throughout the whole process of crack sliding. Note that for $0 < \gamma < 90°$, $\tau'_{12} > 0$ and $\sigma'_2 < 0$.

Once the inequality (2.1) is satisfied and the frictional sliding is activated, the representative slit is in Mode-II loading for which only K_{II} stress-intensity factor is nonzero. At some point the elastic energy release rate $G(\theta) = K_{II}^2/E_0$ (E_0 being the Young's modulus of the intact material) will reach a critical value in a plane at an angle θ_c to the original crack. The critical value of the elastic energy release rate corresponds to the critical value of the tensile hoop stress $\sigma_{\theta\theta}$ in the vicinity of the crack tip. Regardless of the interpretation, the original crack will at this point abruptly sprout a curvilinear wing crack at each tip, making an angle $\theta_c \sim 70°$ with the crack direction. After a short initial curving, the kinked wings will align themselves with the dominant compressive stress σ_1 and become relatively straight as depicted in Fig. 2. The exact trajectory of the wing cracks can be determined by the maximization of $\sigma_{\theta\theta}$. In this phase of rock deformation, the macroscopic inelastic strains result from the coupled effects of frictional sliding and opening of the tensile wing cracks. In other words, the opening by wedging is opposed by the material intrinsic resistance to the wing crack propagation and by the sliding friction of the material against itself.

An exact derivation of the stress intensity factors at the tips of the curvilinear wing cracks involves singular integral equations not lending themselves to rigorous analytical methods of solution. An effective numerical scheme for the solution of these equations was developed in [8]. For a kinked crack with straight wings (Fig. 5b), a closed-form but approximate analytical estimates of the stress intensity factors at the tips A and A' was suggested in [4] and elaborated further in [1]. Having in mind the relative insensitivity of wings to the actual direction and even size of the original slit, it is sufficient to consider a representative kinked crack sketched in Fig. 5b. The original slit is at an angle 45° with respect to the principal macrostresses σ_1 and σ_2. The slightly curved wing cracks are approximated in the sequel by straight lines collinear with the direction of the principal compressive macrostress σ_1.

The heterogeneity of the rock, i.e. inhomogeneous distribution of fracture strength across the volume, has a strong influence on the shape of the crack. Thus, the nicely curved wings (Fig. 2), obtained from theoretical analyses assuming, in accordance with the linear fracture mechanics, the homogeneity of the matrix material, are never observed in natural rocks formations or even experimental rock specimens. Consequently, simplifying the wing crack geometry for the modeling purposes is more than justified. In this note the approximate expressions for K_I, K_{II} contained in [1] will be followed since they furnish good estimates for both small and large wing lengths.

Consider a representative crack configuration depicted in Fig. 5b. Then, according to HORII and NEMAT-NASSER [1], the expressions for the K_I, K_{II} factors at the wing tips reduce to

$$K_I = \frac{\sqrt{2}c}{\sqrt{\pi(L+L^*)}}\tau_{\text{eff}} + \sigma_2\sqrt{\pi L}, \qquad K_{II} = -\frac{\sqrt{2}c}{\sqrt{\pi(L+L^*)}}\tau_{\text{eff}}, \tag{2.2}$$

where L^* is included to render K_I and K_{II} nonsingular when $L \to 0$. The constant L^* can be computed from the condition that the stress intensity factors (2.2) reduce to the solution by COTTERELL and RICE [16] for the kink initiation. In the present case ($\gamma = 45°$) it follows that

$$\frac{L^*}{c} = \frac{32}{9\pi^2[\sin(\pi/8 + \sin(3\pi/8)]^2} = 0.21. \tag{2.3}$$

Numerical computations performed in [1] of the stress intensity factors for a sliding crack of the actual geometry demonstrate a surprising accuracy of the approximate expressions (2.2). This yields another argument in favor of the introduction of the simplified, straight-winged crack instead of an actual curvilinear crack, to make the present model tractable.

The stress intensity factors at the wing tips A and A' can be computed in terms of tractions acting on the initial crack faces (stress-driven crack) or in terms of the opening displacement u (Fig. 5b) imposed at the roots of the wing cracks (displacement-driven crack). The formulas (2.2) were derived along the lines of the first approach. Alternatively, the K_I factor, for instance, computed from a given slip displacement u, takes the following form, [17]

$$K_I' = \frac{G_0\sqrt{2}}{2(1-\nu_0)}\frac{u}{\sqrt{2\pi(L+L^{**}}}\tau_{\text{eff}} + \sigma_2\sqrt{\pi L/2}, \tag{2.4}$$

where L^{**} plays the same role as L^* in Eqs. (2.2) and was found to be $(L^{**}/c) = (\pi^2/32)(L^*/c) = 0.065$. The first term on the right-hand side of

Eq. (2.4) reflects the contribution of wedging while the second one defines the resistive role of the lateral confining pressure. It is obvious that Eqs. $(2.2)_1$ and (2.4) represent the same quantity whenever the sliding activation condition (2.1) is satisfied. This equivalence will be used in Appendix to make a comment on a certain statement contained in [17].

To calculate the length of the kinked extension for prescribed remote stresses a fracture criterion is necessary. Among several fracture criteria examined in the relevant literature the most frequently used ones are:

1. *The maximum energy release rate criterion* which states that crack branching traces a path along which the strain energy release rate G attains a critical value G_{IC}

$$G = G_{IC} \quad \text{or} \quad K_I^2 + K_{II}^2 = K_{IC}^2, \tag{2.5}$$

where K_{IC} is the fracture toughness of the material.

2. *The maximum tensile stress criterion* which states that crack kinking follows the plane of maximum normal stress. This can be expressed as

$$K_I = K_{IC}, \tag{2.6}$$

since the Mode-II loading does not produce any normal stress on the plane of the crack.

According to the literature studies the normal stress criterion (2.6) is most common and will be used in the present analysis.

3. Constitutive model

For the assumed microcracking mechanism and the representative crack configuration it follows directly that the nonlinear axial strain can primarily be attributed to the sliding on preexisting cracks. The lateral strain, however, can be traced both to the sliding and opening of the wing cracks and is, therefore, more pronounced than the axial shortening of the specimen. This fact is corroborated by existing experimental data for hard rocks such as granite (e.g. [18]). The same conclusion is not always true for concrete (cf. [19]) and may be questionable for porous rocks as well. The faces of the sliding crack were assumed to remain in contact throughout the entire process of deformation. Therefore, the microstructural origins of rock dilatancy under compressive stresses are, in the proposed model, the result of crack opening displacements of the wing cracks.

A basic premise underlying the present analysis is that the inelastic behaviour of rocks at low lateral pressures results solely from the irreversible process of progressive damage. Plastic effects observed in polycrystalline rocks, when high lateral pressures are applied, are not included in the present analysis. It is assumed that representative cracks (Fig. 5b) develop from the preexisting cracks, and no nucleation of new material defects is allowed in the course of deformation process. This is pertinent to the cleavage-1 cracks according to the ASHBY'S [20] classification. Such cracks are typical of brittle rocks in low confinement compression tests.

Consider a dilute distribution of N representative sliding cracks per unit area. Interaction between the microcracks is neglected for it is shortly before, or at the apex of the $\sigma - \varepsilon$ curve that the crack interaction begins to play a dominant role (e.g. [21], [22]). Consequently, the overall strains will be estimated by a simple average of the contributions of individual cracks.

It should be mentioned that there are ways to include interactions among the neighbouring cracks. A rather rigorous way of tackling this problem is to determine the stress intensity factors at the tips of interacting pairs of cracks, or infinite rows of cracks, similarly as in [1]. However, the exact derivation of the stress intensity factors for interacting cracks, even of simplified geometry, poses an extremely complex mathematical challenge. Approximate methods, such as the one in [23], may to some extent cure the situation, and make the resulting equations workable in practical applications. An alternative way is to resort to the so-called effective continua methods, such as the self-consistent scheme (see for example [24], [25]) or the double-embedding method [26] in which the crack interaction effects are indirectly accounted for through the effective continuum. This, in turn, involves the solution of the kinked crack evolution in an anisotropic elastic matrix, which is not yet available. The present model is a qualitative study of the sliding crack growth in monotonic compressive stress fields, and of its influence on the brittle deformation of rocks. As such, it does not aspire to incorporate highly complex crack interaction effects.

Assume further that strains remain small, thus the total strain tensor may be decomposed into the strain due to initial compaction of pores $\boldsymbol{\varepsilon}^c$, elastic strain $\boldsymbol{\varepsilon}^0$, and the average damage strain $\boldsymbol{\varepsilon}^*$ which accounts for the inelastic deformation of the preexisting microcracks, i.e.

$$\boldsymbol{\varepsilon} = \boldsymbol{\varepsilon}^c + \boldsymbol{\varepsilon}^0 + \boldsymbol{\varepsilon}^*. \tag{3.1}$$

The strain due to enforced initial compaction of pores is not included in

the subsequent considerations, although this can be done without major changes, if required. For example, using the self-consistent method it is possible to estimate the effective elastic constants of a solid with uniformly distributed spherical voids as functions of porosity. Furthermore, knowing the change of porosity as a function of stresses, it becomes possible to determine the evolution equation for the change in the elastic parameters as the void density parameter is decreased.

In the formulation of a damage model the effect of symmetry has to be taken into account. In a rock specimen weakened by a random population of many preexisting cracks, there is an equal chance for a slanted representative crack to be oriented either at $\gamma = 45°$ or $\gamma = 135°$ (Fig. 6). In other words, there are just as many cracks at an angle 45° as there are cracks at 135°. In this case, considering pairs of cracks, the shear macrostrains vanish, and the only non-vanishing components of the inelastic strain tensor are the axial shortening ε_1^* and the lateral expansion ε_2^*.

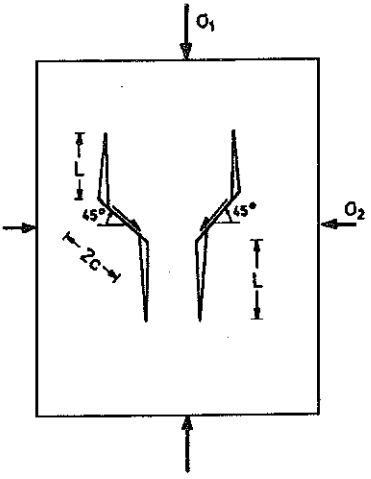

FIG. 6.

Inelastic strains attributed to frictional sliding (segment BC in Fig. 4). The stress σ_{0c} at the onset of relative frictional slip of the faces of a closed rectilinear slit (Fig. 5a) is determined from the slip activation condition (2.1) as

$$\sigma_{0c} = \frac{2\tau_c - \sigma_2(1+\mu)}{\mu - 1}. \tag{3.2}$$

The inelastic strains associated with the crack sliding can be computed fairly easily provided that the slip displacement u is assumed uniform (constant)

along the preexisting flaw PP'. Using the conventional divergence theorem, the strains due to discontinuities of the displacement (in any mode) along a surface ($-a \leq l \leq a$) with normal n can be written as

$$\varepsilon'_{ij} = \frac{1}{2} N \int_{-a}^{a} \left(n'_j u'_i + n'_i u'_j \right) dl, \tag{3.3}$$

where N is the crack density (number of cracks in a unit volume, or area) and the integration extends over the entire surface (length, in this case) of the discontinuity. Since the rectilinear crack remains closed throughout the entire process of sliding, it follows from Eq. (3.3) that in the local (crack-attached) coordinate system $(1', 2')$ the macrostrains ensuing from the frictional sliding are

$$\varepsilon'_{11} = \varepsilon'_{22} = 0, \qquad \varepsilon'_{12} = \varepsilon'_{21} = N \int_{0}^{c} u'_1 \, dl = Nuc. \tag{3.4}$$

Note that N is the property of the specimen reflecting the degree of damage that exists prior to the considered loading. The average slip u is, as noticed by NEMAT-NASSER and OBATA [17], nothing else but the Mode-II crack opening displacement averaged over the crack length $2c$, i.e.

$$u = \frac{1}{2c} \int_{-c}^{c} \frac{4(1-\nu_0^2)}{E_0} \sqrt{c^2 - l^2} \tau_{\text{eff}} \, dl = \frac{1-\nu_0^2}{E_0} \pi c \tau_{\text{eff}}. \tag{3.5}$$

In the global coordinate system (1, 2) the strain tensor due to frictional sliding takes the form

$$\varepsilon^*_{ij} = \varepsilon'_{12} \begin{bmatrix} -1 & 0 \\ 0 & 1 \end{bmatrix} = f \frac{1-\nu_0^2}{E_0} \pi \tau_{\text{eff}} \begin{bmatrix} -1 & 0 \\ 0 & 1 \end{bmatrix} \qquad (i,j = 1,2), \tag{3.6}$$

where $f = Nc^2$ is now a parameter characterizing crack size and density.

Strains due to kinked microcracks (segment CF in Fig. 4). The relative sliding of the preexisting crack faces is now coupled with the growth of tension wing cracks. The stress level σ'_{0c} indicating the kink initiation is defined from the fracture criterion (2.6) or (3.15) for $L \to 0$. After simple rearrangements it follows that

$$\sigma'_{0c} = \frac{1}{\mu - 1} \left[K_{IC} \frac{\sqrt{2\pi L^*}}{c} - \sigma_2(\mu + 1) + 2\tau_c \right]. \tag{3.7}$$

In the considered phase, a rigorous determination of the crack opening displacements requires non-trivial computational efforts. Therefore, an alternative route will be followed allowing to obtain the stress-strain relationships in a simpler way.

The expression for the complementary energy density ψ stored in the elastic damaged solid consists of two terms ψ^0 and ψ^*. The first term represents the energy of the virgin elastic material and is a sole function of the stress tensor $\boldsymbol{\sigma}$. The second term characterizes the change in the complementary energy due to the microcrack appearance. It depends on the stress tensor, the microcrack number and sizes, i.e.

$$\psi(\boldsymbol{\sigma}, N, L) = \psi^0(\boldsymbol{\sigma}) + \psi^*(\boldsymbol{\sigma}, N, L). \tag{3.8}$$

The complementary energy density is supposed to be the Gibbs' potential, i.e. a scalar-valued function of the stress tensor whose derivative with respect to the stress component determines the corresponding strain component

$$\varepsilon_{ij} = \left.\frac{\partial \psi}{\partial \sigma_{ij}}\right|_{L=\text{const}}. \tag{3.9}$$

For N non-interacting cracks in a unit area the complementary energy density (3.8) takes the form

$$\psi = \frac{1}{2} S^0_{ijkl}\sigma_{ij}\sigma_{kl} + 2N \int_0^L \frac{K_I^2 + K_{II}^2}{E_0} dl, \tag{3.10}$$

where $\mathbf{S}^0$ is the fourth-order elastic compliance tensor of the intact material.

Inserting (2.2) into (3.10) and performing some cumbersome though analytical integration, the expression for the inelastic part of the Gibbs' potential becomes

$$\begin{aligned}\psi^* = \frac{2N}{E_0}\Bigg\{\Bigg\{&\frac{c^2}{\pi}\left[(1-\mu)^2\sigma_1^2 - 2(1-\mu^2)\sigma_1\sigma_2 + (1+\mu^2)\sigma_2^2\right] \\ &- \frac{4}{\pi}c^2\tau_c\left[(\mu-1)\sigma_1 + (\mu+1)\sigma_2 - \tau_c\right]\Bigg\}\ln\left(\frac{L}{L^*}+1\right) \\ &+ \frac{1}{2}\pi L^2\sigma_2^2 + \sqrt{2}c\left[(\mu-1)\sigma_1\sigma_2 + (1+\mu)\sigma_2^2 - 2\tau_c\sigma_2\right] \\ &\times\left[\sqrt{L(L+L^*)} - \frac{1}{2}L^*\ln\left(\frac{\left(\sqrt{L+L^*}+\sqrt{L}\right)^2}{L^*}\right)\right]\Bigg\}.\end{aligned} \tag{3.11}$$

Introduce now the following normalization:

$$\tilde{L} = L/c, \qquad \tilde{L}^* = L^*/c, \qquad \tilde{L}^{**} = L^{**}/c. \tag{3.12}$$

Then, the inelastic strains in the considered two-dimensional case are:

Axial:

$$\varepsilon_1^* = \frac{\partial \psi^*}{\partial \sigma_1} = \frac{4f}{\pi E_0} \ln\left(\frac{\tilde{L}}{\tilde{L}^*} + 1\right) \left[\sigma_1(1-\mu)^2 - \sigma_2(1-\mu^2) + 2(1-\mu)\tau_c\right] + \frac{2\sqrt{2}}{E_0} f(\mu - 1) \times \left[\sqrt{\tilde{L}(\tilde{L}+\tilde{L}^*)} - \frac{\tilde{L}^*}{2} \ln\left(\sqrt{\frac{\tilde{L}}{\tilde{L}^*} + 1} + \sqrt{\frac{\tilde{L}}{\tilde{L}^*}}\right)^2\right] \sigma_2. \tag{3.13}$$

Lateral:

$$\varepsilon_2^* = \frac{\partial \psi^*}{\partial \sigma_2} = \frac{4f}{\pi E_0} \left\{ \ln\left(\frac{\tilde{L}}{\tilde{L}^*} + 1\right) \left[\sigma_1(\mu^2 - 1) + \sigma_2(1+\mu^2)\right] + \frac{1}{2}(\pi L)^2 \sigma_2 + \left[\sqrt{\tilde{L}(\tilde{L}+\tilde{L}^*)} - \frac{\tilde{L}^*}{2} \ln\left(\sqrt{\frac{\tilde{L}}{\tilde{L}^*} + 1} + \sqrt{\frac{\tilde{L}}{\tilde{L}^*}}\right)^2\right] \times \sqrt{2\pi} \left[\frac{1}{2}(1-\mu)\sigma_1 - 2(1+\mu)\sigma_2 - \tau_c\right] \right\}. \tag{3.14}$$

The next step consists in eliminating the crack length from the analysis by relating it with the stresses through the fracture condition. As already mentioned, the maximum tensile stress criterion (2.6) is used for this purpose, thus

$$K_I = -\sqrt{\frac{2}{\pi}} \frac{c}{\sqrt{L + L^*}} \tau_{\text{eff}} + \sigma_2 \sqrt{\pi L} = K_{IC}. \tag{3.15}$$

This leads to a rather complicated algebraic equation

$$(\tilde{L} + \tilde{L}^*)^2 \left(\pi \tilde{L} \sigma_2^2 - \frac{K_{IC}^2}{c}\right)^2 - \tilde{L}(\tilde{L} + \tilde{L}^*)(2\tau_{\text{eff}}\sigma_2)^2 - (\tilde{L} + \tilde{L}^*)\frac{2}{\pi c}(2\tau_{\text{eff}} K_{IC})^2 + \left(2\frac{\tau_{\text{eff}}}{\pi}\right)^2 = 0, \tag{3.16}$$

from which it is possible to compute numerically the crack length $\tilde{L}$ for current values of σ_1 and σ_2. Combining Eq. (3.16) with Eqs. (3.13) and (3.14) the nonliner stress-strain relations are then obtained making this micromechanical model complete.

4. Application: uniaxial compression

Consider the case of unconfined axial compression ($\sigma_1 < 0$, $\sigma_2 = 0$). The inelastic strains (3.6) in the phase of crack sliding reduce to

$$\varepsilon_{ij}^* = \frac{1-\nu_0^2}{E_0}\pi f\left(\frac{1}{2}(\mu-1)-\tau_c\right)\begin{bmatrix} -1 & 0 \\ 0 & 1 \end{bmatrix}, \qquad (i, j = 1, 2). \tag{4.1}$$

The relation (3.16) between the stresses and the wing crack length in the kinking phase takes the following explicit form

$$\tilde{L} + \tilde{L}^* = \frac{2c}{\pi K_{IC}^2}\left[\frac{1}{2}(\mu-1)\sigma_1 + \tau_c^2\right]^2. \tag{4.2}$$

Inserting Eq. (4.2) into (3.13) and (3.14) we arrive at the closed-form stress--strain relations

$$\varepsilon_1^* = \frac{4f}{\pi E_0}\ln\left\{\frac{2c}{\pi K_{IC}^2\tilde{L}^*}\left[\frac{1}{2}(\mu-1)\sigma_1 - \tau_c\right]^2\right\} \times \left[(1-\mu)^2\sigma_1 + 2(1-\mu)\tau_c\right], \tag{4.3}$$

$$\begin{aligned}\varepsilon_2^* = {} & -\varepsilon_1^* - \frac{4\sqrt{2}}{E_0} f\left[\frac{1}{2}(\mu-1)\sigma_1 - \tau_c\right] \\ & \times \left(\sqrt{\left(\frac{4c^2}{\pi^2 K_{IC}^2}\left[\frac{1}{2}(\mu-1)\sigma - \tau_c\right]^2 - \frac{2c\tilde{L}^*}{\pi}\right)}\frac{1}{K_{IC}}\left[\frac{1}{2}(\mu-1)\sigma_1 - \tau_c\right]\right. \\ & -\frac{\tilde{L}^*}{2}\ln\left\{\sqrt{\frac{2c}{\pi\tilde{L}^*}}\frac{1}{K_{IC}}\left[\frac{1}{2}(\mu-1)\sigma_1 - \tau_c\right]^2\right. \\ & \left.\left.+\sqrt{\frac{2c}{\pi K_{IC}^2\tilde{L}^*}\left[\frac{1}{2}(\mu-1)\sigma_1 - \tau_c\right]^2 - 1}\right\}\right).\end{aligned} \tag{4.4}$$

In order to test the capability of these equations in duplicating the behaviour of a real rock we seek to fit the experimental data obtained by Zoback and Byerlee [18] for the uniaxial loading of Westerly granite cylinders. The material parameters for Westerly granite were taken from [18, 4, 17], and are listed below:

initial Young's modulus	$E^0 = 56500\,\text{MPa},$
initial Poisson's ratio	$v^0 = 0.25,$
friction coefficient (constant)	$\mu = 0.5,$
fracture toughness	$K_{IC} = 1.0\,\text{MPa}\sqrt{\text{m}},$
ultimate strength	$\sigma_{uc} = 204\,\text{MPa},$
initial average length of preexisting flaw	$c = 5 \cdot 10^{-4}\,\text{m},$
initial flaw density parameter	$f = 0.2,$
cohesive shear strength (constant)	$\tau_c = 10.0\,\text{MPa}.$

The limits separating the elastic and inelastic responses reduce to

$$\sigma_{0c} = \frac{2\tau_c}{\mu - 1} = 40\,\text{MPa}, \tag{4.5}$$

$$\sigma'_{0c} = \frac{2}{\mu - 1}\left(K_{IC}\sqrt{\frac{\pi \tilde{L}^*}{2c}} + \tau_c\right) = 122.7\,\text{MPa}.$$

The final graph of stress vs. axial and lateral strains is presented in Fig. 7. Since the initial closure of preexisting voids was not accounted for in the present model, the computed axial $\sigma - \varepsilon$ curve was shifted from the origin 0 by the strain obtained from the intercept of the linear portion of the experimental curve with the ε-axis. The remarkable agreement with the experimental data, although pleasing, should be taken with caution because the experimental results are for a cylindrical specimen whereas the model

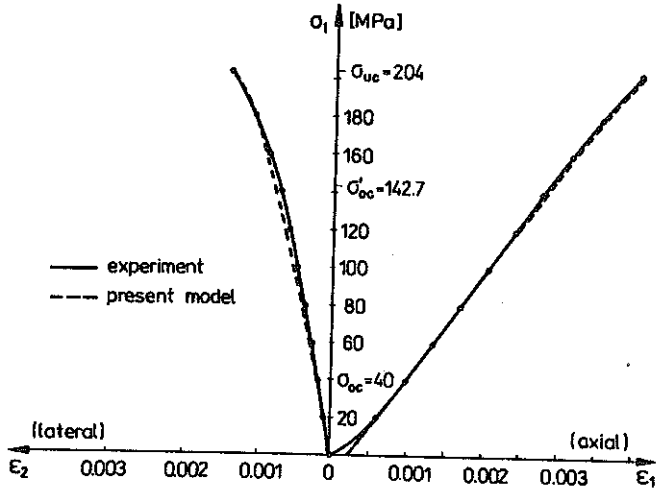

FIG. 7.

is two-dimensional. Nevertheless, this simple model does predict several important features of the brittle response of granite. For instance, the overall trends are well preserved for both curves, and the lateral inelastic strain is larger than its axial counterpart. Note that all material parameters used for computations are realistic and are documented in the referenced literature.

It is anticipated, however, that a constitutive model of this type, based on the instability of a single crack, will not be able to predict the cooperative type of final failure. The cooperative failure is characteristic of a rock specimen subjected to large confinements. In such a case microcrack interaction is the dominant mechanism in formation of a crack band and must be, as such, properly accounted for in future modeling efforts.

5. Comments on unloading and brittle-to-ductile transition

Assuming that the ultimate strength of the specimen was not exceeded, the final phase of the deformation process consists in unloading (segment DE of the stress-strain curve in Fig. 4). In the course of quasi-static unloading the material response is initially linearly elastic up to a point E. In general, the axial elastic modulus in the region DE will be slightly reduced in comparison with its initial value measured from the slope of the segment AB. This results from the fact, that following the loading cycle to the point D, the rock specimen becomes more compliant due to microcracking. However, for the assumed representative kinked microcrack oriented at 45 degrees with straight vertical wings parallel to the axial compressive stress σ_1, the axial elastic modulus in unloading (DE) is assumed to be virtually the same as for the segment AB of the stress-strain curve. During the elastic unloading all the preexisting slits are locked and the wing cracks remain open. At the point E the backsliding commences. The condition for the initiation of backsliding can be found elsewhere (e.g. Jaeger and Cook [27], p. 331). In the case of uniaxial compression ($\sigma_1 \neq 0$, $\sigma_2 = 0$), the reverse sliding occurs if the drop in the applied remote stress $\Delta\sigma_1$ exceeds the value

$$\Delta\sigma_1 \geq \frac{2\mu}{1+\mu}\sigma_1^{\max}, \tag{5.1}$$

where $\sigma_1^{\max}$ denotes the maximum compressive stress applied to the specimen in loading (point D in Fig. 4). The permanent (residual) strain that remains in the specimen after a complete unloading (i.e. when the externally

applied stress is reduced to zero) is commonly attributed to the imperfect crack closure and, to the lesser extent, to the plastic strains if the lateral confinement was present. Determinations of the permanent strains were considered to be beyond the scope of the initial phase of the model development. Detailed analysis of the unloading process is the objective of current studies and will be reported separately.

Another outstanding feature yet to be analyzed and incorporated into this model is the brittle-to-ductile transition observed in rock deformation processes. The brittle-to-ductile transition point is the ratio of the lateral to axial stress beyond which failure is preceded by substantial plastic deformation. The lateral pressure supresses the unstable growth of the wing cracks leading to the appearance of plastic zones around the tips of the preexisting cracks PP', Fig. 5b. Analytical description of the transition from brittle to ductile behaviour of a rock is a complex problem involving studies of the relative contributions of energies dissipated in brittle and ductile regimes. HORII and NEMAT-NASSER [1] suggested that the appropriate parameter defining this transition is the so-called ductility ratio:

$$\Delta = \frac{K_{IC}}{\tau_Y \sqrt{\pi c}}, \tag{5.2}$$

where K_{IC} is the fracture toughness and τ_Y is the yield stress for a considered rock. For low porosity rocks like granite application of Eq. (5.2) may be quite useful. The ductility ratio for the Westerly granite was found to be $\Delta \approx 0.05$. According to the graphs in [1] this value indicates that the transition from brittle to ductile mode of deformation proceeds without entering the so-called transition mode, where the brittle and ductile effects are coupled. Thus, brittle and ductile response can be considered separately with no account for the interaction effects. This, certainly, facilitates the analysis since, in order to incorporate the ductile response of granite, the concept of the Dugdale crack (cf. [28]) could be used. In order to determine the strains resulting from plastic deformation around the preexisting crack tips it is necessary to compute the size of the plastic zone. Preliminary computations show that this can be done in analytical form.

6. CLOSING REMARKS

The analytical model discussed in this paper presents, in essence, a feasibility study needed to ascertain the effort required to formulate a microme-

chanically-based constitutive model for characterizing rocks in *in-situ* conditions. The ultimate objective of this research program is to improve the constitutive laws used as input for specialized computer softwares for analyses of real problems in the mechanics of rock masses. Therefore, simplicity of formulation is deemed a vital condition for this stage of the research. It was also mandatory from the experimental point of view to ensure clear and unambiguous identification of all constituent parameters of the analytical model.

Based on the work contained herein it can be concluded that the model is rather straightforward for simple proportional loading conditions. However, in the case of arbitrary non-proportional and/or cyclic loadings the analytical model will become increasingly complex. The unilateral constraints imposed by a crack on the displacement field seems to be the major problem source. Unlike the plastic slip, the crack opening displacement essentially depends on the sign of the normal stress. Consequently, analyses considering loading paths characterized by change of normal stresses from tensile to compressive and vice versa will, by their very nature, involve discontinuous changes of material stiffnesses. The ensuing complexities in large scale computations may reach substantial levels.

The main thrust of the work summarized in this report was directed towards the determination of dominant mechanisms of irreversible changes in microstructure of low-porosity rocks. For one of these mechanisms, i.e. a kinked crack in an elastic medium, the fundamental relations between the kinematic variables and corresponding stresses on the microscale are discussed in detail. Assuming that the selected mechanism captured the main aspects of physics of the deformation process, a string of simplifying assumptions were introduced to enhance the tractability of the proposed model. For example, in departure from rigorous micromechanical models, the proposed model considers only a single representative crack.

Some aspects of the overall deformation process, most notably a proper characterization of the unloading and softening regimes, were barely mentioned here. In addition, the brittle-to-ductile transition must be fully and thoroughly investigated.

The kinked crack mechanism is commonly accepted as suitable for compact crystalline rocks. For more porous rocks, models emphasizing cracks emanating form compressed spherical voids may be more adequate. Thus, other cracking mechanisms should be given appropriate attention when constructing a reasonably general model of rock deformation.

Despite all the limitations listed, the introductory research effort summarized in this paper clearly indicates the capabilities of micromechanical modeling in description of brittle rock deformation and failure.

APPENDIX

The expressions $(2.2)_1$ and (2.4) represent the Mode-I stress intensity factors computed for the winged crack of Fig. 5b regarded as stress- or displacement-driven crack, respectively. The essential difference between these two expressions is contained in the latter term responsible for the effect of lateral stresses σ_2. The K_I factor computed in the presence of a concentrated gap (imposed crack opening displacement) is for the crack length L. Having in mind that compressive stress field σ_2 acts normally to the wing crack axis, its contribution to Eq. (2.4) is $\sigma_2\sqrt{\pi(L/2)}$. On the other hand, if K_I is computed for a stress-driven crack, the crack length is $2L$ and the term in question shows up in $(2.2)_1$ as $\sigma_2\sqrt{\pi L}$. It is claimed in [17] that *"this difference is quite small due to the fact that the tension cracks grow in the maximum compressive stress direction"*. Consequently, *"in order to ensure a consistent formulation without loss of accuracy"* it is suggested in [17] that the term $\sigma_2\sqrt{\pi L}$ be used in both formulas.

As already mentioned in Sec. 2, the expressions $(2.2)_1$ and (2.4) define the same stress intensity factor, thus we can use this identity to single out the sliding displacement u:

$$u = 2c\frac{1-\nu_0}{G_0}\left[\sqrt{2\frac{\tilde{L}+\tilde{L}^{**}}{\tilde{L}+\tilde{L}^{*}}}\,\tau_{\text{eff}} + \sigma_2\pi\sqrt{\tilde{L}(\tilde{L}+\tilde{L}^{*})}\left(1-\frac{\sqrt{2}}{2}\right)\right]. \tag{A.1}$$

Following the suggestion of NEMAT-NASSER and OBATA [17], the second term in square brackets of (A.1) would disappear meaning that the amount of slip is entirely independent of the lateral confinement σ_2, and almost independent of the wing length $\tilde{L}$. This conclusion does not seem to be justified.

ACKNOWLEDGEMENT

This work was supported by the Polish Committee for Scientific Research under the Grant no. 310149101: *Thermomechanics of Damage and Phase Transformations in Materials.*

References

1. H.Horii and S.Nemat-Nasser, *Brittle failure in compression: splitting, faulting and brittle-ductile transition*, Phil. Trans. Roy. Soc. London, **319**, 1549, pp. 337–374, 1986.
2. W.F.Brace and E.G.Bombolakis, *A note on brittle crack growth in compression*, J. Geophys. Res., **68**, pp. 3709–3713, 1963.
3. M.L.Kachanov, *A microcrack model for rock inelasticity, Part II: Propagation of microcracks*, Mech. of Materials, **1**, pp. 29–41, 1982.
4. W.C.Moss and Y.M.Gupta, *A constitutive model describing dilatancy and cracking in brittle rock*, J. Geophys. Res., **87**, pp. 2985–2998, 1982.
5. C.G.Sammis and M.F.Ashby, *The failure of brittle porous solids under compressive stress states*, Acta Metall., **34**, pp. 511–526, 1986.
6. P.Steif, *Crack extension under compressive loading*, Eng. Fracture Mech., **20**, 3, pp. 463–473, 1984.
7. J.M.Kemeny and N.G.W.Cook, *Micromechanics of deformation in rocks*, Toughening Mechanisms in Quasi-Brittle Materials, S.P. Shah [Ed.], pp. 155–188, Kluwer Acad. Publishers, 1991.
8. S.Nemat-Nasser and H.Horii, *Compression-induced nonplanar crack extension with application to splitting, exfoliation, and rockburst*, J. Gephys. Res., **87**, B8, pp. 6805–6821, 1982.
9. D.Fanella and D. Krajcinovic, *A micromechanical model for concrete in compression*, Eng. Fracture Mech., **29**, pp. 49–66, 1988.
10. D.Gross, W.Becker and M.Basista, *A simple mesostructural model for damage-induced inelasticity of brittle materials*, Yielding, Damage and Failure of Anisotropic Solids, J.P. Boehler, ed., Mech. Engng Publications Ltd, pp. 681–692, London 1990.
11. D.E.Chitty and S.E.Blouin, *Background on fracture of rock*, Report for DNA/SPWE Fracture Mechanics Meeting at Arizona State University, Tempe, July 1991.
12. C.H.Sondergeld and L.H.Estey, *Source mechanism and microfracturing during uniaxial cycling of rock*, Pure and Applied Geophysics, **120**, pp. 151–160, 1982.
13. T.Yanagidani, S.Ehara, O.Nishizawa, K.Kusunose and M.Terada, *Localization of dilatancy in Westerly granite under constant uniaxial stress*, J. Geophys. Res., **90**, pp. 6849–6858, 1985.
14. N.P.Cannon, E.M.Schulson, T.R.Smith, H.J.Frost, *Wing cracks and brittle compressive fracture*, Acta Metall. Mater., **38**, pp. 1955–1962, 1990.
15. D.Krajcinovic, *Damage mechanics*, Mech. of Materials, **8**, pp. 117–197, 1989.
16. B.Cotterell and J.R.Rice, *Slightly curved or kinked cracks*, Int. J. Fracture, **16**, pp. 155–169, 1980.
17. S.Nemat-Nasser and M.Obata, *A microcrack model of dilatancy in brittle materials*, J. Appl. Mech., **55**, pp. 24–35, 1988.

18. M.D.ZOBACK and J.D.BYERLEE, *The effect of cyclic differential stress on dilatancy in Westerly Granite under uniaxial and triaxial conditions*, J. Geophys. Res., **80**, pp. 1526–1530, 1975.

19. D.KRAJCINOVIC, M.BASISTA and D.SUMARAC, *Micromechanically inspired phenomenological damage model*, J. Appl. Mech., **50**, pp.305–311, 1991.

20. M.F.ASHBY, *Micromechanisms of fracture in static and cyclic failure*, Fracture Mechanics, R.A. Smith ed., Pergamon Press, Oxford, pp. 1–27, 1979.

21. A.HANSEN, S.ROUX and H.J.HERRMANN, *Rupture of central-force lattices*, J. Physique, **50**, pp. 733–744, 1989.

22. D.KRAJCINOVIC and M.BASISTA, *Rupture of central-force lattices-revisited*, J. Physique I, **1**, pp. 241–245, 1991.

23. M.L.KACHANOV, *Elastic solids with many cracks – a simple method of analysis*, Int. J. Solids Struct., **23**, pp. 23–43, 1987.

24. R.HILL, *A self-consistent mechanics of composite materials*, J. Mech. Phys. Solids, **13**, pp. 223–227, 1965.

25. B.BUDIANSKY and R.J.O'CONNELL, *Elastic moduli of cracked solid*, Int. J. Solids Struct., **12**, pp. 81–97, 1976.

26. Z.HASHIN, *The differential scheme and its application to cracked materials*, J. Mech. Phys. Solids, **36**, pp. 719–734.

27. J.C.JAEGER and N.G.W.COOK, *Fundamentals of Rock Mechanics*, 2nd Edition Chapman and Hall, London 1976.

28. M.F.KANNINEN and C.H.POPELAR, *Advanced Fracture Mechanics*, Oxford University Press, New York 1985.

POLISH ACADEMY OF SCIENCES
INSTITUTE OF FUNDAMENTAL TECHNOLOGICAL RESEARCH.

Received September 10, 1993.